On a numerical subgrid upscaling algorithm for Stokes–Brinkman equations

O. Iliev[a], Z. Lakdawala[a], V. Starikovicius[b]

[a] *Fraunhofer ITWM, Fraunhofer-Platz 1, D-67663 Kaiserslautern, Germany*
{*iliev, lakdawala*}*@itwm.fhg.de*
[b] *Vilnius Gediminas Technical University, Vilnius, Lithuania*
vadimas.starikovicius@sc.vgtu.lt

Abstract

This paper discusses a numerical subgrid resolution approach for solving the Stokes-Brinkman system of equations, which is describing coupled flow in plain and in highly porous media. Various scientific and industrial problems are described by this system, and often the geometry and/or the permeability vary on several scales. A particular target is the process of oil filtration. In many complicated filters, the filter medium or the filter element geometry are too fine to be resolved by a feasible computational grid. The subgrid approach presented in the paper is aimed at describing how these fine details are accounted for by solving auxiliary problems in appropriately chosen grid cells on a relatively coarse computational grid. This is done via a systematic and a careful procedure of modifying and updating the coefficients of the Stokes-Brinkman system in chosen cells. This numerical subgrid approach is motivated from one side from homogenization theory, from which we borrow the formulations for the so called cell problem, and from the other side from the numerical upscaling approaches, such as Multiscale Finite Volume, Multiscale Finite Element, etc. Results on the algorithm's efficiency, both in terms of computational time and memory usage, are presented. Comparison with solutions on full fine grid (when possible) are presented in order to evaluate the accuracy. Advantages and limitations of the considered subgrid approach are discussed.

Keywords: Stokes-Brinkman equations, subgrid approach, multiscale problems, numerical upscaling.

1. Introduction

The demands of the industry regularly pose new challenging problems to applied mathematics. In many cases the existing algorithms do not work, and new specialized algorithms for classes of industrial problems are demanded. Developing algorithms for a class of filtration problems (filtering solid particles out of liquid) is discussed in this paper. Numerical simulations, when they can be performed, allow significant reduction in time and costs for design of new filter elements with proper flow rate - pressure drop ratio. The CFD simulations assisting this design are characterized by three peculiarities:

- The filtering porous layers are usually manufactured with certain variations in the weight (i.e., in porosity and permeability), and consistently with this, accuracy of 5 to 8 per cent for the pressure drop across a filter element is the target of the simulations.
- High accuracy for the flow velocity within a filter element is not required, as long as the pressure drop over the complete filter element is properly computed.
- 30-36 simulations with different flow rates and different viscosities have to be performed for each geometry to evaluate the performance of the filter element at different flow and temperature conditions.

Our aim is to account for these peculiarities, in order to develop efficient algorithm for this particular class of problems.
In the case of liquid filtration, the flow is usually laminar, and at low and moderate temperatures it is slow (due to higher viscosity), and it is described by the Stokes-Brinkman system of equations (see, e.g., [22] and references therein):

$$\underbrace{\rho\frac{\partial\vec{u}}{\partial t}-\nabla\cdot(\tilde{\mu}\nabla\vec{u})}_{Stokes}+\overbrace{\tilde{\mu}\tilde{\mathbf{K}}^{-1}\vec{u}+\underbrace{\nabla p=\tilde{\vec{f}}}}^{Darcy} \tag{1}$$
$$\nabla\cdot\vec{u}=0,$$

where

$$\tilde{\mu}=\begin{cases}\mu & \text{in } \Omega_f\\ \mu_{eff} & \text{in } \Omega_p\end{cases}\quad \tilde{\vec{f}}=\begin{cases}\vec{f}_{NS} & \text{in } \Omega_f\\ \vec{f}_B & \text{in } \Omega_p\end{cases}\quad \tilde{\mathbf{K}}^{-1}=\begin{cases}0 & \text{in } \Omega_f\\ \mathbf{K}^{-1} & \text{in } \Omega_p\end{cases}$$

Here $\vec{u}, p$ stand for velocity and pressure respectively, $\rho, \tilde{\mu}$ and $\mathbf{K}$ denote the density, viscosity, and the permeability tensor of the porous medium, respectively.

The Stokes equations (cf. [4, 19]) govern the flow in pure fluid regions. The Brinkman equations (cf. [7]) are introduced as an extension to the Darcy model for the flow in porous media for the case of highly porous media (note, that porosity of the non-woven filtering media, which is our primary interest, is often more than 0.9). Concerning the hierarchy of the models for the porous media flow, we refer to the recent review in [10]. The Stokes-Brinkman system is used to describe the coupled flow in plain and in porous media. For its justification, see [18]. Some details on modeling and simulation of flow through oil filters using the Stokes-Brinkman and Navier-Stokes-Brinkman systems of equations can be found in [30, 15, 22].

Most of the filters are characterized by complicated shape of the filtering medium/media (e.g. pleats and/or perforated porous layer/s), and/or by complicated shape of the filter element housing (e.g. ribs, perforated inner cylinder, etc.). Some examples are illustrated in Figure 1. The existing commercial (e.g. Gambit, http://www.fluent.de) and academic (e.g. Netgen, http://www.hpfem.jku.at/netgen/) grid generators, are often unable to generate grids in such complicated domains, even when an experienced researcher is the user. In many cases, the generated grid is either of very bad quality, or the grid cannot be generated at all. Most engineers working on the design of filter elements are not experienced in grid generation techniques, and an alternative approach is needed in this case. The grid generation procedure works robustly if one restricts to voxel or brick elements, and therefore we chose this approach. A pre-processor based on the level set method (c.f. [1]) is used to process given CAD data for attaining the assembly of a filter housing in the form of a computational domain (union of voxel or brick control volumes). Different conventions can be used to characterize a control volume by a certain material type. Most commonly, the material type of its center point is assigned to the whole CV, or the dominating material type in the control volume is assigned to it. This grid generation approach is stable, and a fluid flow solver using the aforementioned grid generator is successfully used for a variety of industrial applications (c.f. [16, 13, 14]). However, in general, such types of grids contain a large number of elements: in certain cases, a very fine grid has to be used to accurately resolve all geometrical features, what in turn results in a large number of elements.

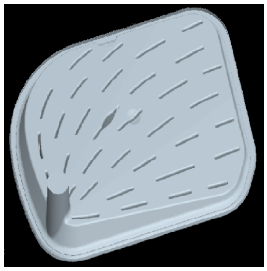

Figure 1: Some examples of the complex geometries and complicated shapes of the filtering media.

For the cases where the geometrical features are at different scales, various approaches for multiscale problems can be adopted to provide an increase in the efficiency of the flow algorithms. Recall that the Darcy equation can be rigorously derived as a macroscopic model for flow in porous media, in the case of periodic or statistically homogeneous porous media. The Stokes system of equations at pore scale (c.f. [27]) is the basis of these derivations. Depending on the the porosity, Allaire [6] homogenizes the Stokes problem to the Darcy or the Brinkman system. Clearly, the homogenization approach is very restrictive, i.e. it can be used only for periodic or statistically homogeneous porous media, and for the Stokes (and not for Navier-Stokes) system at the pore scale. The homogenization theory works in the case of scale separation, and it allows for a drastic reduction of the computational costs: only one auxiliary problem is solved in a periodicity cell on the fine scale, its solution is post-processed to compute the coefficients of the macroscopic equation, and the macroscopic equation is further solved at the coarse scale. The coefficients of the macroscopic equation in this case are called upscaled, homogenized, or effective coefficients. For the cases when the homogenization theory does not work, its ideas can still be imported to the numerical upscaling approaches, such as the Multiscale Finite Element Method (MsFEM) [23], the Mixed MsFEM, [3], the Multiscale Finite Volume Method [21, 8, 5] and the Subgrid Method [26, 24, 9, 17]. Another approach which serves as a building block for numerical upscaling procedures, is the volume averaging approach combined with the Representative Elementary Volume (REV) concept (cf. [12]). Unlike the homogenization theory, this approach is not based on asymptotic expansions, but on the volumetric averaging of functions and their derivatives. For example, if a block of porous medium is large enough (i.e. representative), its Darcy permeability is defined from the

requirement that the macroscopic pressure drop is equal to the microscopic pressure drop computed by solving the Stokes problem at the pore level.

In the case of saturated flow in porous media, homogenization is studied either in connection with the mesoscopic and macroscopic Darcy models (upscaling elliptic equation with oscillating coefficients to macroscopic elliptic equation, i.e. upscaling Darcy to Darcy (cf. [29])), or in connection with impermeable porous matrix and fluid flow in the (connected) pore space, i.e. upscaling Stokes to Darcy (cf. [27]). The Authors could not find articles on upscaling Stokes-Brinkman system at mesoscale to some macroscale system of equations, except a recent work concerning numerical study of homogenization of Brinkman equations [36].

In this paper, we discuss a subgrid upscaling algorithm for the Stokes-Brinkman system of equations. We also solve Navier-Stokes regimes in certain cases, working in the context of iterative upscaling, but this issue is not discussed here. The subgrid approach was recently used in some simpler applications, namely the Darcy problem (single phase flow in porous medium) (cf. [25], [32], [9]). In the subgrid approach, one solves a problem on a coarser grid, but accounts for the unresolved geometrical features by solving local auxiliary problems on the underlying finer grid in all (or some selected) coarse cells. This paper deals with applying a similar approach in solving the incompressible Stokes-Brinkman equations in highly complex domains. The numerical solution for such systems is computationally expensive in terms of memory usage and computational time, and the subgrid approach is developed to compute a reliable pressure drop at reasonable computational costs.

The remainder of the paper is organized as follows. A one-scale model (it can be also called single grid model), i.e. the Stokes-Brinkman system of equations, is described in 2. It includes a short description of the Finite Volume discretization, and the Chorin projection method employed for solving the model numerically. Section 3 is devoted to introducing the concept of *quasi-porous* coarse cells and to the description of the subgrid algorithm for the Stokes-Brinkman system. Due to lacking theoretical results for the upscaling of the Stokes-Brinkman system, we perform a numerical study of this approach. In Section 4, we present validation results for the developed subgrid upscaling procedure. Results from numerical simulation of industrial filters are also presented in this Section. Finally, some conclusions are drawn.

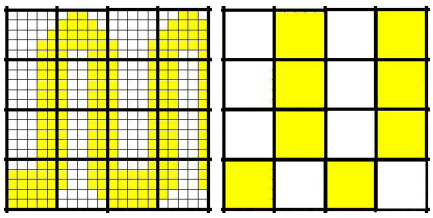

Figure 2: Illustration of an example of quasi-porous cell/s where the fine scale resolves the geometrical details(the white cells represent pure fluid region; yellow cells on the left picture correspond to porous media, on the right pictures the yellow cells are of so called quasi-porous type).

2. Governing equations and the single grid algorithm

The fine scale system includes the Stokes-Brinkman system of equations (1) in a complicated 3D domain Ω, consisting of porous, solid and fluid subdomains, i.e. $\Omega = \Omega_p \cup \Omega_s \cup \Omega_f$.
The flow domains considered in the current work are of different geometric characteristics, as shown in Figure 1. The governing equations are solved subject to the following boundary conditions which are typical in filtration problems. At the inlet of the free flow region, a velocity profile is specified. At the outlet, zero pressure is imposed. No slip boundary conditions are imposed elsewhere on walls.
The coarse scale system also employs the Stokes-Brinkman system of equations but with an upscaled permeability for specified quasi-porous coarse cells, such that the Equation (1) is replaced with

$$\rho\frac{\partial\vec{u}_0}{\partial t} - \nabla\cdot(\tilde{\mu}\nabla\vec{u}_0) + \tilde{\mu}\tilde{\mathbf{K}}_{eff}^{-1}\vec{u}_0 + \nabla p_0 = \tilde{\vec{f}}_0 \tag{2}$$

where $\vec{u}_0$, p_0 denote the coarse scale velocity and pressure respectively. Here $\tilde{\mathbf{K}}_{eff}$ stands for the effective upscaled permeability, and the details of its computations are given in Section 3.

Single grid algorithm

The computational domain is a connected union of control volumes (CVs), where each CV is a brick. The equations are discretized by the finite volume method. A collocated arrangement of the unknowns $\vec{u}$ and p is used, i.e. the unknowns are assigned to the centers of CVs. The Chorin method [2] for the Navier-Stokes equations [19, 4], along with a proper modification for

Stokes-Brinkman case [22], is used as a projection method decoupling velocity and continuity equations (note, the Chorin projection for unsteady Stokes problem is very close to the preconditioners for unsteady Stokes problem suggested in [35]) . The fractional time step discretization scheme can be written as

$$(\rho\vec{u}^* - \rho\vec{u}^n) + \tau(-D + B)\vec{u}^* = \tau G p^n \tag{3}$$

$$\left(\rho\vec{u}^{n+1} - \rho\vec{u}^*\right) + \tau(B\vec{u}^{n+1} - B\vec{u}^*) = \tau(Gp^{n+1} - Gp^n) \tag{4}$$

$$G^T \rho\vec{u}^{n+1} = 0 \tag{5}$$

where $D\vec{u}$ denote the operator corresponding to the discretized viscous terms. The particular form of these operators depend on the spatial discretizations. G and G^T denote the discretized gradient and divergence operator. $B\vec{u}$ denotes the Darcy operator in the momentum equations whereas the superscript $^{k+1}$ and ^{k} denotes the new and the old time level, respectively.

The sum of Equations (3) and (4) results in an implicit discretization of the momentum equations. Equation (3) is solved with respect to the velocities using the old value of the pressure gradient, thus obtaining a prediction for the velocity. To solve the second equation for pressure correction, one takes the divergence from it and uses the continuity equation. The resulting equation is a Poisson type equation for the pressure correction which is discussed in detail in [22].

3. Subgrid Algorithm

In this section, a subgrid algorithm for the Stokes-Brinkman system is discussed. The goal is to develop an algorithm which computes not only the pressure drop across a filter element on a relatively coarse grid, but also preserves the pressure drop accuracy corresponding to a finer grid. The idea is to account for a subgrid resolution on the coarse grid by solving proper local auxiliary problems on the fine grid, and using their solution for calculating the permeability of quasi-porous coarse cells. In fact, solving local problems in order to account for the fine scale features is a common approach for numerical upscaling methods, such as MsFEM, MSFV, etc.

For a given computational domain, Ω, we consider a fine grid and a coarse grid. The fine grid is assumed to contain all important geometrical details,

but solving the Stokes-Brinkman system of equations on this grid is memory and CPU intensive, or even impossible. As discussed in the Introduction, a material type (in our case fluid, solid, or porous) is assigned to each fine grid cell during the pre-processing stage. The coarse grid has a size, such that the problem is solvable at acceptable computational costs. Each coarse cell is a union of fine grid cells. Each coarse cell is considered, and the coarse grid cells containing mixture of solid & liquid, or liquid & porous, or solid & porous, or solid & liquid & porous fine grid cells, are defined as *quasi-porous* cells, for which effective (upscaled) permeability tensors have to be computed. It is assumed that the Stokes-Brinkman equations describe the flow on the fine grid and on the coarse grid. In the latter case, the coarse scale permeability is the effective (upscaled) permeability tensor $\tilde{\mathbf{K}}_{eff}$. Currently, the diagonal permeability tensor i.e. $\tilde{\mathbf{K}}_{eff} = \{K_{11}, K_{22}, K_{33}\}$ is considered, and the extension to the full tensor is ongoing work.

The computation of upscaled coefficients requires solving the local fine scale problem in some coarse grid cells. Two approaches are considered:

- The upscaled (effective) permeability is computed for each individual *quasi-porous* coarse grid cell. Similar to the block-permeability upscaling procedure for single phase flow in porous media (cf. [31]), the localization boundary conditions are specified on its boundary (see discussion below for more details; possible oversampling is also discussed below);

- Alternatively, certain union of coarse cells is considered as a single block for which auxiliary problem is solved on the underlying fine grid. Thereafter, the upscaled (effective) permeability is assigned to each of the coarse cells forming the block. This approach is motivated by the Representative Elementary Volume concept, where a reasonably large heterogeneous (at a fine scale) volume has to be considered, in order to assign effective (upscaled) coarse scale properties to it.

The upscaling approach considered here is similar to the one used by Durlofsky et al.[11] for the elliptic pressure equation, and to the approach considered and justified in the recent article [36]. The Darcy law is used there to compute the effective (upscaled) permeability of a coarse cell from the averaged fine grid pressure and velocity. In general, different types of (localization) boundary conditions can be specified for the auxiliary problems. Periodic boundary conditions suit very well for periodic geometries. The pressure drop in one

of the directions, and no flow (or symmetry) in the remaining directions, are often used. In the homogenization approach considered in [6], the constant velocity at infinity is prescribed as the boundary condition for the auxiliary problem. It is well known that the choice of the localization boundary conditions plays an important role in numerical upscaling methods, and we are currently working on comparing results for different (localization) boundary conditions. This work, however, will be reported elsewhere. Currently, the following local boundary conditions are considered for the auxiliary problems for the Stokes-Brinkman system:

- inflow velocity U_{in} at the inlet face (for the current direction);
- outflow b.c. at the outlet face: $p = P_{out}$, $\frac{\partial \mathbf{u}}{\partial \mathbf{n}} = \mathbf{0}$;
- symmetry b.c. elsewhere.

The auxiliary problems are solved for each direction d. Next, the average inlet pressure P_{in} is computed from the local fine scale solution and is used to obtain the effective permeability K_{dd} of the quasi-porous cell in direction d from the Darcy law [12, 36]:

$$K_{dd} = \frac{\mu U_{in} L_d}{P_{in} - P_{out}}, \tag{6}$$

where L_d is the distance between the inlet and outlet faces. The use of this approach is motivated by the fact that we are interested in computing the accurate pressure drop of the complete filter element. By calculating the effective permeability using Equation (6), we account for the resistance of the geometrical features which were otherwise unresolved on the coarse computational grid. Note, that in [36], this approach for computing the effective permeability was carefully and systematically compared to the standard formula from the homogenization literature (e.g., [6, 27]), and a very good agreement was found.

Implementation of the subgrid method
Here, we discuss the Subgrid method. The algorithm consists of four main components:

1. Selection of the quasi-porous coarse cells

2. Solution of the auxiliary problems with a fine grid resolution on selected coarse cells with boundary conditions, as specified above

3. Computation of the effective permeabilities for the quasi-porous cells

4. Solution of the full coarse scale problem, using the calculated effective permeabilities.

Step (1) includes a mapping of each coarse cell onto the underlying union of fine grid cells. If the composition of fine grid cells contains a mixture of fluid and/or porous and/or solid, it is marked with a 'quasi-porous' flag. Alternatively, at this stage, a block of coarse cell can be specified as quasi-porous.

Step (2) defines the local auxiliary problem on the quasi-porous coarse cells. The same space discretization, i.e. the finite-volume method, is considered on the fine scale and a solution is computed. Note, that additional layers can be added to a quasi-porous cell. In upscaling techniques, this is known as *oversampling*. Mostly, the domain is extended by a 'bordering ring' with fine grid cells. We consider additional fine scale 'bordering layers' of type 'fluid' on a specified boundary. The number of additional layers is denoted by l in the next section. If $l = 0$, it is a purely local auxiliary solve. If $l = 1$, it means that the auxiliary problem is solved in coarse cell extended with one fluid layer in the specified direction, as shown on Figure 5(d).

Step (3) assigns the effective permeability tensors to the coarse cells, post-processing the auxiliary fine grid solution computed from step (2). Steps (2) and (3) are performed for every quasi-porous cell selected in step (1). Note, that in the case when the coarse cells/blocks are periodic (e.g., this is the case when each coarse quasi-porous block contains one pleat), the auxiliary problem needs to be solved once for each type of quasi-porous coarse cells. Furthermore, the once computed permeabilities are reused in the computations with the same geometry, but with a different flow rate or viscosity (recall that 30-36 simulations have to be performed for each filter element geometry).

Step (4) includes the standard algorithm which solves the Stokes-Brinkman system of equations on the coarse grid.

Remark 1: (1) The same solver is used for solving global coarse scale problem and auxiliary problems on the fine grid. (2) Different stopping criteria can be specified for the local and for the global problems.

Remark 2: If the number of quasi-porous blocks is too large, Steps (2)-(3) become the most time consuming part of the solution procedure. Implementation is modular-based and the subgrid algorithm is parallelized, so that the auxiliary problems are distributed to different processes for faster computations.

4. Results and validation

The results from numerical simulations are presented in this section. The performed simulations can be divided into three groups:

- Validation for thin porous layer and for the upscaled permeability computation (Subsections 4.1 and 4.2). Stokes flow around a spherical obstacle is considered in the Subsection 4.1 to check the influence of the used voxel grid as well;
- Numerical study of Brinkman to Brinkman upscaling. As mentioned earlier, the upscaling approaches for Stokes and for Darcy flows are theoretically considered in the literature, and due to the lack of theoretical results for the upscaling of Brinkman equation, we perform a numerical study here (we refer also to the recent paper [36]);
- Simulations for the industrial filters with complicated geometry of the porous media (perforated layer in one case, pleats in the other case), and complicated geometry (solid mesh supporting the perforated layer in one case, and complicated filter element housing in the other case).

Whenever possible, the results from the simulations with the upscaled equations are compared with the results obtained solving the fine grid problem for the same geometry. This is the methodology employed for the validation of the developed subgrid algorithm. It should be noted that the single grid simulations have already been validated against measurements(c.f. [30]).

The computations and CPU time measurements were performed on dedicated node of Fraunhofer ITWM cluster 'Hercules' with dual Intel Xeon 5148LV ('Woodcrest') processor (2.33 GHz).

4.1. Permeability for a periodicity cell: flow around a sphere

For better understanding of the subgrid algorithm, an example of an auxiliary problem for a quasi-porous coarse cell is considered. Consider a cube

occupied by the fluid with the sphere-shaped solid obstacle inside, as shown in Figure 3. Suppose that we consider a domain which is a periodic arrangement of such cells. Permeability for such a geometry is computed many times via homogenization and other upscaling approaches, and it is also measured (see,e.g., the discussion in [36]). Our goal for solving the Stokes flow in this geometry is twofold. i.) From one side, we want to check if the boundary conditions for the auxiliary cell problems and REV type approach for calculating the upscaled permeability, as described above, gives good results; ii) Additionally, we want to check the influence of the voxel-based discretization grid that is used to discretize the sphere.

The auxiliary problem is solved on the fine grid resolution scale of 0.25mm with the following input data: cube size - $L = 12\,\text{mm}$, with different sized spheres with radius r; inflow velocity $U_{in} = 1.1574\,\text{mm/s}$, $P_{out} = 0\,\text{kg/(mm s}^2)$, density($\rho$) $= 1.0 \cdot 10^{-7}\,\text{kg/mm}^3$, viscosity($\mu$) $= 1.0 \cdot 10^{-4}\,\text{kg/(mm s)}$. Table 4.1 shows the results obtained by our algorithm with permeability computed using Darcy law, denoted by $\mathbf{K}_{Darcy}$. The computed values are compared with the results on unit cell problem reported by Griebel and Klitz [36] and Sangani and Acrivos [34], denoted by $\mathbf{K}_{Cell}$ and $\mathbf{K}_{Experiment}$ respectively. It is observed that the computed results are in good comparison with the cited results. A systematic study on grid resolution was performed, and it concluded that the error reduces with finer grid resolutions where the voxel-based disretization better approximates the solid sphere.

Figure 3: Cube with solid sphere inside. Inlet, outlet and symmetry walls are marked with colors blue, green and red respectively.

r	$\mathbf{K}_{Darcy}$	$\mathbf{K}_{Cell}$ (Griebel, Klitz)	$\mathbf{K}_{Experiment}$ (Sangani, Acrivos)
0.2	1.18×10^{-1}	1.23×10^{-1}	1.23×10^{-1}
0.25	7.34×10^{-2}	7.40×10^{-2}	7.46×10^{-2}
0.3	4.35×10^{-2}	4.46×10^{-2}	4.45×10^{-2}
0.35	2.48×10^{-2}	2.52×10^{-2}	2.52×10^{-2}

Table 1: Comparison of permeability in a 3D array of spheres (cell problem) for different radii

4.2. Channel filter with single porous layer

This example is chosen to be a simplified filter element geometry (parallelepiped) with a thin layer of porous media. The computational domain is $\{(x, y, z) : 0 \leq x \leq 12,\ 0 \leq y \leq 24,\ 0 \leq z \leq 24 \text{ mm}\}$, with a single porous layer $\{(x, y, z) : 4.5 \leq x \leq 5.5,\ 0 \leq y \leq 24,\ 0 \leq z \leq 24 \text{ mm}\}$, as shown in Figure 4. On coarse grids, when the step size of the grid is bigger than the thickness of the layer, the latter can not be correctly resolved. The thickness of the filtering medium is correctly resolved on 0.5 mm grid. However, on grid 2 mm, the pre-processor provides a porous layer with 2 mm thickness (recall that the pre-processor assigns to a grid cell the material type of its center point). Solving problem (1) with $U_{in} = 28.9\,\text{mm/s}$, $\rho = 1.0 \cdot 10^{-7}\,\text{kg/mm}^3$, $\mu = 1.0 \cdot 10^{-4}\,\text{kg/(mm s)}$, and isotropic permeability $K = 1.0 \cdot 10^{-4}\,\text{mm}^2$, we obtain (correct) pressure drop of $28.95\,\text{kg/(mm s}^2\text{)}$ on 0.5 mm grid, and a twice bigger (wrong) value, i.e. $57.9\,\text{kg/(mm s}^2\text{)}$ on 2 mm grid. Note, that the considered flow is essentially one-dimensional one and one can easily find its analytical solution.

Application of the subgrid algorithm for 2 mm coarse and 0.5 mm fine grids gives 144 (12×12) quasi-porous cells, which are all identical in this case, as shown in Figure 5 (a). Solution of the auxiliary problem in X direction gives the value of permeability $K_{11} = 2.0 \cdot 10^{-4}$ (the other components of the permeability tensor are not important in this case). Using the obtained permeability for the quasi-porous cells, we solve the problem on the 2 mm coarse grid, and get the correct pressure drop, i.e. 29.0.

Including additional layers at inlet and outlet

Using 1 mm size for the coarse grid, we get two different geometries of quasi-porous cells in X direction, as illustrated in Figure 5 (b) and (c). Solving auxiliary problems for these geometries gives wrong values of the upscaled permeability in X direction: $K_{11} = 1.60 \cdot 10^{-4}$ for *left* cell and $K_{11} = 2.67 \cdot 10^{-4}$ for *right* cell. This is because the fine porous cells are touching the outlet of auxiliary problem in first case, and the inlet in the second, which does not allow full development of the flow. To deal with this issue, we have an option of adding 'border rings', which are a specified number of layers of fine fluid cells before the inlet and/or outlet of the actual domain in any specified direction. Figure 5 (d) shows the auxiliary problem for the *right* 1 mm cell with 1 additional fluid layer in front of the inlet. Solving this auxiliary problem gives correct value of upscaled permeability: $K_{11} = 2.0 \cdot 10^{-4}$. The

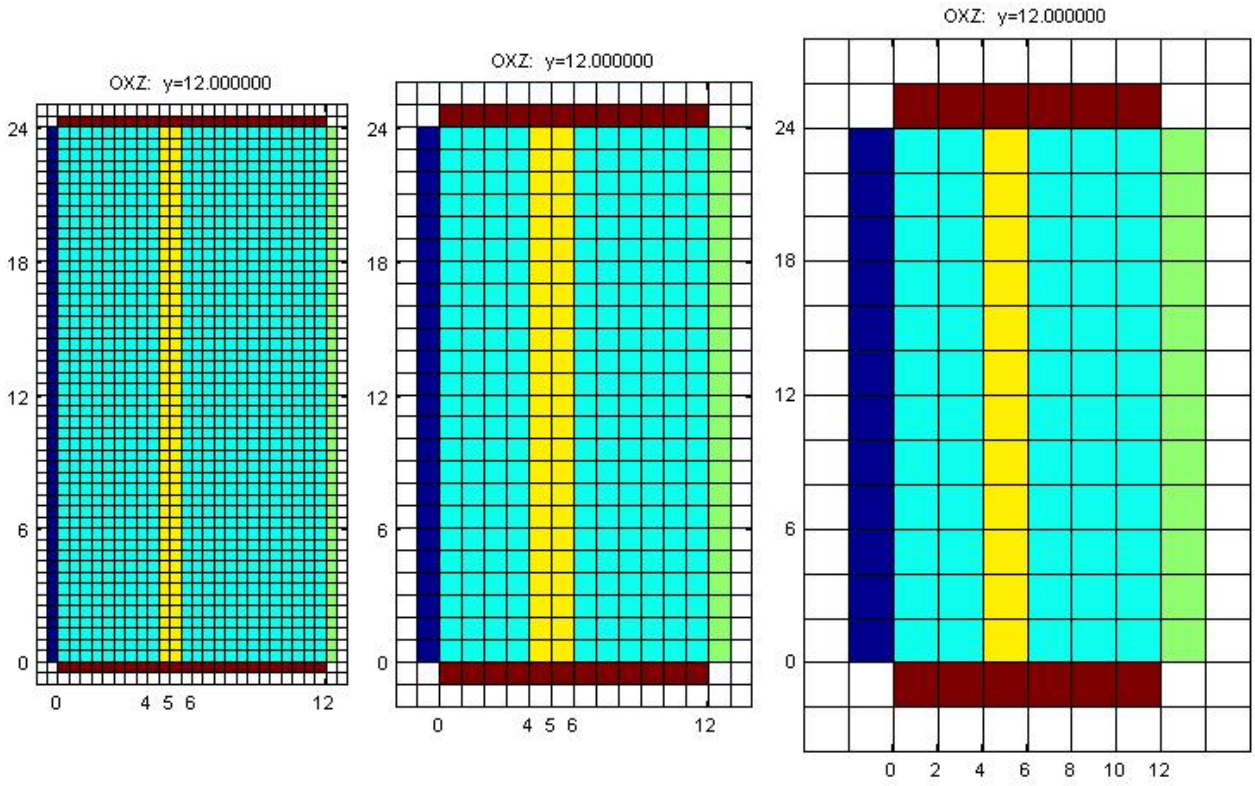

(a) 0.5 mm grid (b) 1 mm grid (c) 2 mm grid

Figure 4: Channel filter with the single porous layer.

same value is obtained for the *left* cell with additional fluid layer behind the outlet. Finally, solving the global problem on the coarse 1 mm grid with the upscaled permeabilities gives correct value of the global pressure drop, i.e. 28.95.

4.3. Channel filter with single porous layer with a hole

As a next example, the same filter geometry is considered as in subsection 4.2 but with $U_{in} = 2.8e-03$ and with a small hole in the porous layer - $\{(x, y, z) : 4.5 \leq x \leq 5.5,\ 10.5 \leq y \leq 11.5,\ 10.5 \leq z \leq 11.5 \text{ mm}\}$. This hole is correctly resolved on 0.5 mm grid. On 2 mm grid, this $1 \times 1 \times 1$ mm hole is exactly in the center of $2 \times 2 \times 2$ mm coarse cell, as illustrated in Figure 6 (a) and (b). Figure 6 (a) is a view along the channel, whereas Figure 6 (b) is a view across the channel. Therefore, as opposed to the previous case, this cell

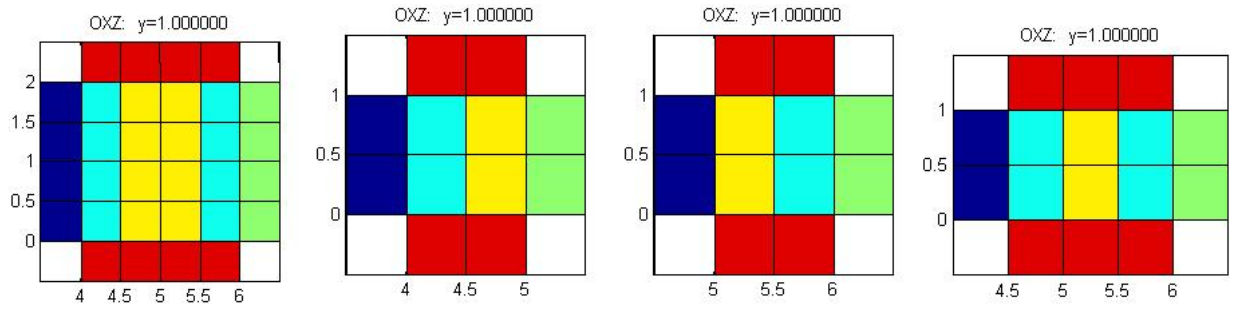

(a) 2 mm (b) 1 mm *left* (c) 1 mm *right* (d) *right* + 1 layer

Figure 5: Auxiliary problems for 2 and 1 mm quasi-porous cells in X direction for channel filter with the single porous layer.

is fluid on 2 mm grid, and the cross section of the hole as well as the thickness of the porous layer are wrongly depicted. On 1 mm grid, all 8 $1 \times 1 \times 1$ mm cells, covering the hole, have a porous center and therefore remain porous, as shown in Figure 6. Hence, 1 mm grid resolution remains the same as shown in Figure 4(b) in Section 4.2.

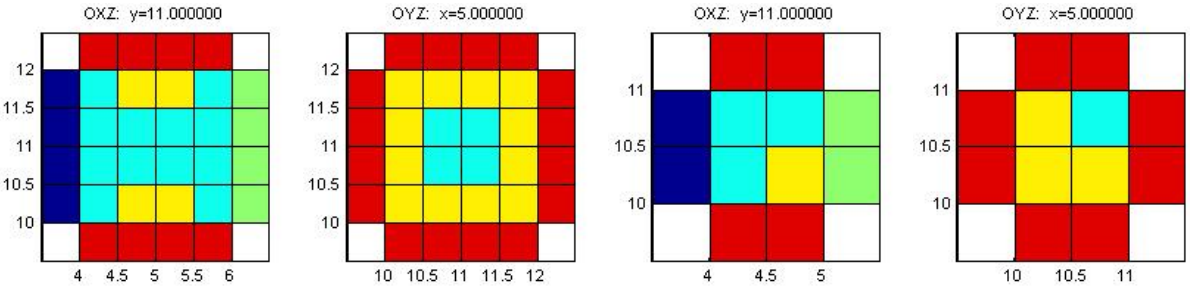

(a) 2 mm (b) 2 mm (c) 1 mm (d) 1 mm

Figure 6: Auxiliary problems for 2 and 1 mm quasi-porous cells in X direction for channel filter with the single porous layer with a hole.

In Table 2, results for the different grid resolutions using the single grid algorithm are presented. On the 2 mm grid, the hole is too big, therefore we get relatively small pressure drop. The grids with step size 0.5 and 0.25 mm resolve the hole exactly (see Figure 6 (b)). Clearly it is expensive to compute accurate solution on a single fine grid, and a subgrid approach is the remedy for efficient simulations.

Next, we discuss the results of the subgrid algorithm for this problem. In

Grid resolution	Number of CVs	Memory [MB]	CPU time [s]	Pressure drop [kg/(mm s^2)]
2 mm	864	0.80	2	0.00353
0.5 mm	55296	33.73	206	0.01486
0.25 mm	442368	247.1	2489	0.01669

Table 2: Simulation results for channel filter with single porous layer with a hole.

Table 3, we present the results obtained for 2 mm coarse and several (0.5, 0.25 mm) fine scale combinations. Calculations were done with different number of additional fluid layers l used for the solution of the auxiliary problems. We show the computed values of the upscaled permeability K_{11} for the quasi-porous cell with hole and the global pressure drop dP. Also, the CPU time T_{SG} of preprocessing step only is given, because the subsequent solution of system on the coarse 2 mm grid was taking less than 10 seconds for all shown cases. The maximal memory used by the solver in all cases was 1.08 MB (coarse grid solver + upscaled permeability tensors).

Scales	l	K_{11}	T_{SG}	dP
2/0.5 mm	0	0.0226	14	0.0168
2/0.5 mm	2	0.0272	140	0.0156
2/0.5 mm	4	0.0273	203	0.0156
2/0.25 mm	0	0.0198	155	0.0177
2/0.25 mm	2	0.0217	345	0.0172
2/0.25 mm	4	0.0218	516	0.0171

Table 3: Simulation results for channel filter with single porous layer with hole (obtained with Subgrid algorithm). l is the number of additional fluid layers. K_{11} is the upscaled permeability obtained for quasi-porous cell with hole. T_{SG} is CPU time of preprocessing step. dP is the obtained global pressure drop.

4.4. Channel filter with periodic porous layer

The next example is a channel/parallelepiped filter $\{(x, y, z) : 0 \leq x \leq 75,$ $0 \leq y \leq 15,\ 0 \leq z \leq 15$ mm$\}$ with porous layer $(30 \leq x \leq 45)$ consisting of two porous materials with a periodic structure, as shown in Figure 7.

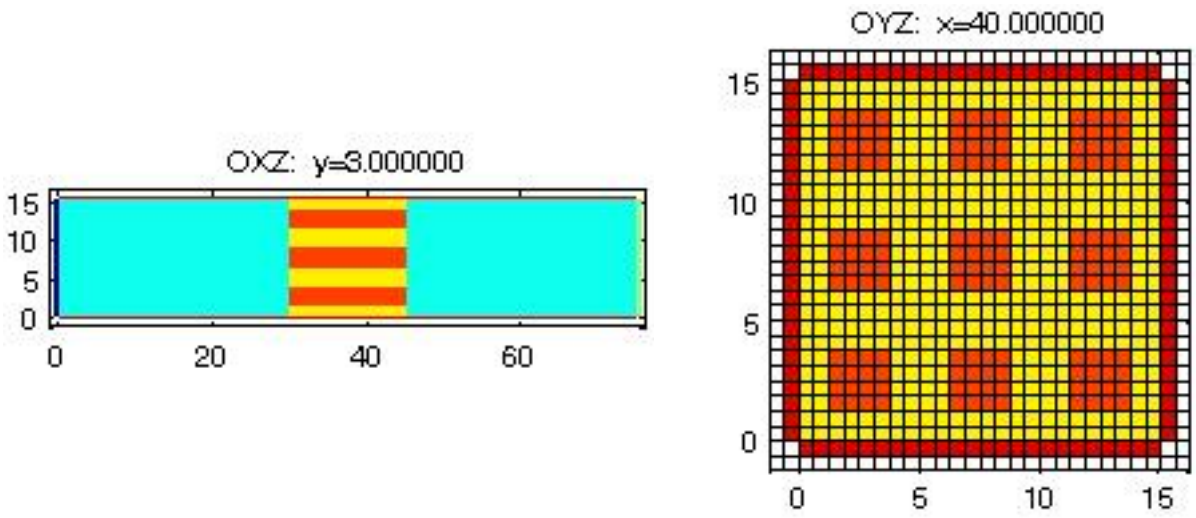

(a) (b) $(3 \times 3\text{: } 8 \times 8)$

Figure 7: Channel filter with two peridic porous layers (3×3) represented in yellow and red. (a) and (b) represent two different cross sections of $x - z$ axis and $y - z$ axis of the filter.

The first porous material(in yellow) in Figure 7 has permeability $K = 1.0 \cdot 10^{-4}\,\mathrm{mm}^2$. The second porous material (in red color) is more permeable with permeability $K = 2.0 \cdot 10^{-4}\,\mathrm{mm}^2$. The problem (1) is solved with the same parameters as before.

For Figure 7, the results on the fine scale, $24 \times 24 \times 24$, are obtained. The pressure drop $dP = 80.005$ is obtained in 9.42 seconds. The grid is further coarsened 8 times, such that $8 \times 8 \times 8$ fine cells comprises of one coarse cell and the results using the coarse and the fine grid are obtained using the subgrid algorithm. The results obtained are $dP = 80.008$ in 4.55 seconds.

Figure 8 (a) shows a geometry with a fine scale discretization containing $30 \times 30 \times 30$ finite volumes. Compared to Figure 7(b), there is 1.5% more of the less permeable porous material and we expect a greater pressure drop across the filter element. The single grid algorithm results in $dP = 86.21$ in 21.65 seconds. The grid is then coarsened 3 times, such that $10 \times 10 \times 10$ fine cells constitutes one coarse cell. Using both, fine and coarse scales, the subgrid algorithm results in $dP = 86.21$ in 8.39 seconds.

Figure 8 (b) illustrates five, instead of three, periods of the second type of the

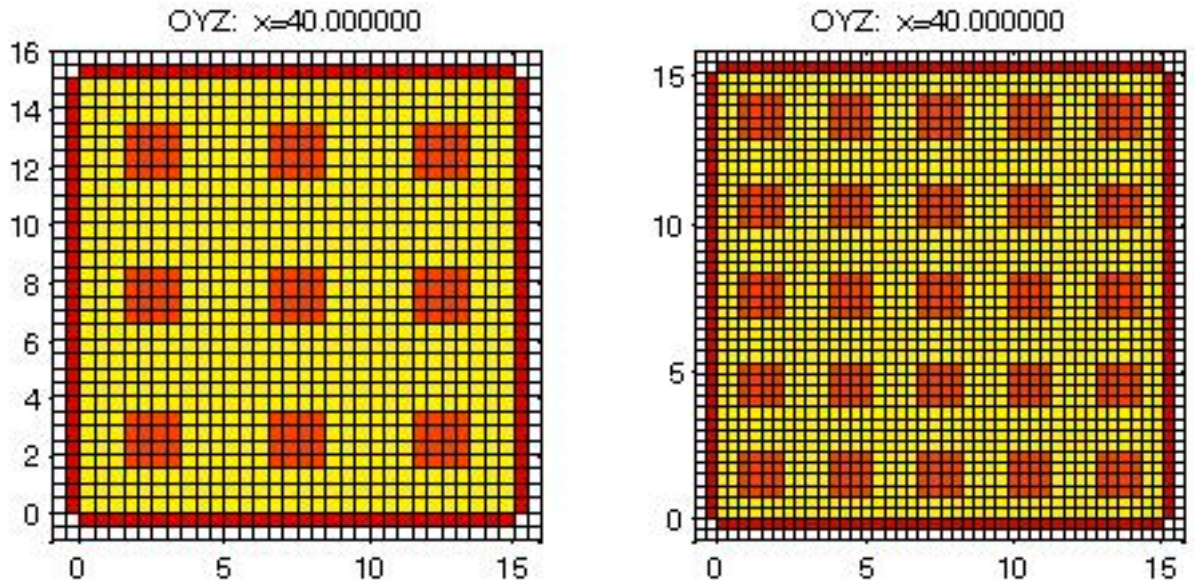

(a) (3x3: 10x10) (b) (5x5: 8x8)

Figure 8: Channel filter with peridic porous layer.

porous material which has a higher permeability. The geometry compares with the geometry shown in Figure 7. We see that pressure drop $dP = 80.012$ is obtained in 52.67 seconds using the single grid algorithm with fine scale discretization of $40 \times 40 \times 40$ cells. The coarse discretization contains $5 \times 5 \times 5$ cells. Subgrid algorithm results in $dP = 80.015$ in 21.82 seconds.

Lastly, instead of three, periods of the second type of the porous material which has a higher permeability for the geometry that compares with the geometry shown in Figure 8. We see that the pressure drop $dP = 86.25$ is obtained in 124.96 seconds using the single grid algorithm with fine scale discretization of $50 \times 50 \times 50$ cells. The coarse discretization contains $5 \times 5 \times 5$ cells. The subgrid algorithm results in $dP = 86.22$ in 41.23 seconds.

4.5. Channel filter with the combi layers

The next example is chosen to serve the needs of the design of new generation of filters as shown in Figure 9 (a) . It should be noted that oil filters are often equipped with a so called bypass option. The bypass prevents the oil to filter through the porous media, especially at cold temperatures (i.e. high viscosity). The idea behind such design was to prevent the destruction of

the filter due to the high pressure in such cases. Instead, the oil bypasses the filtering medium via some small pipe. Obviously, the bypassed oil is not filtered in this situation. Alternatively, the new league of filters are designed without the bypass option, but with an additional layer of a fine perforated filter layer that allows the oil to flow through the holes at cold temperatures. Additionally, a coarse filter layer in the form of a solid mesh is added to filter out the large particles. With the support of the numerical simulations, the size of the holes and the distance between the two porous layers are designed such that most oil flows through the porous part of the first layer at high temperature, and not through the holes. It is common understanding that the porous layers are the primary cause of the pressure drop across the filter. This is true only when the filter element is designed in a way that there is enough space between the inlet(bottom) and the porous layer, and between the porous layer and the outlet(top). Therefore, we study this filter in a simplified geometry, i.e. a simple channel geometry as shown in Figure 9 (b). The considered filter element is parallel piped $\{(x, y, z) : 2 \leq x \leq 67, -11 \leq y \leq -2, -67 \leq z \leq -2 \text{ mm}\}$ with two filtering porous layers and a supporting solid mesh between them, as shown in Figure 10 (b). Additionally, the first porous layer ($-8 \leq y \leq -7$) has a set of 6×6 holes, as shown in Figure 10 (b), where each hole is a cube: $1 \times 1 \times 1\,\text{mm}$, as illustrated in Figure 11 (a).
When using the 2 mm resolution, the mesh layer is not captured at all and both porous layers have the wrong, doubled thickness, on this grid: $-8 \leq y \leq -6$ and $-6 \leq y \leq -4$, respectively. The 1 mm grid represents the channel and all three layers (including the solid mesh) correctly except for the holes in the first porous layer. As shown in Figure 11, all 4 $1 \times 1 \times 1\,\text{mm}$ cells, covering the hole, have a porous center and therefore are represented as porous in 1 mm grid. The 0.5 and 0.25 mm grids resolve the whole geometry of the filter exactly.

System 1 is solved with the following flow parameters: $U_{in} = 3.944773\,\text{mm/s}$, $\rho = 1.0 \cdot 10^{-7}\,\text{kg/mm}^3$, $\mu = 1.0 \cdot 10^{-4}\,\text{kg/(mm s)}$, isotropic permeability of first porous layer, $K = 4.2 \cdot 10^{-5}\,\text{mm}^2$, and isotropic permeability of second porous layer, $K = 7.5 \cdot 10^{-4}\,\text{mm}^2$. Note that in this test case the main flow is in Y direction.

In Table 4, the results of single grid algorithm for different grid resolutions are presented. It is due to the aforementioned errors in the geometry resolution for 2 to 1 mm grids, that the resulting pressure drop is over estimated. As one

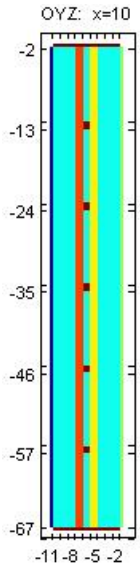

(a) (b)

Figure 9: (a) A real industrial filter with multiple porous media layers. (b) Channel filter with the multiple porous layers. A simplified channel filter of the industrial filter to understand real processes.

goes to finer resolutions, i.e. 0.5 to 0.25 mm, the geometry is resolved more accurately resulting in a more accurate pressure drop. However, computation on the finer grids come with the cost of extensive CPU time consumption and memory usage.

Next, we present the results from the subgrid algorithm for this problem. 2 mm resolution is too coarse to be used even as the coarse scale, where the 1 mm scale seems to be an appropriate choice. Alternatively, a bigger block of coarse cells can be used as an auxiliary problem for computing permeability. As discussed above, for 1 mm grid the only cells, which will be detected as 'quasi-porous', are the cells covering the holes in first porous layer (see Figure 11 (a)). It means that the total of $4 \times 6 \times 6 = 144$ quasi-porous cells will be detected. As can be seen from Figure 11 (c) and (b), solving the auxiliary problem for the main component of upscaled permeability tensor - K_{22}, the flow will be almost aligned with the Y axis and we can expect good results even without the use of full permeability tensor. It is also clear that the additional fluid layers are needed for the auxiliary problems.
In Table 5 we present the results obtained for two coarse/fine grids combi-

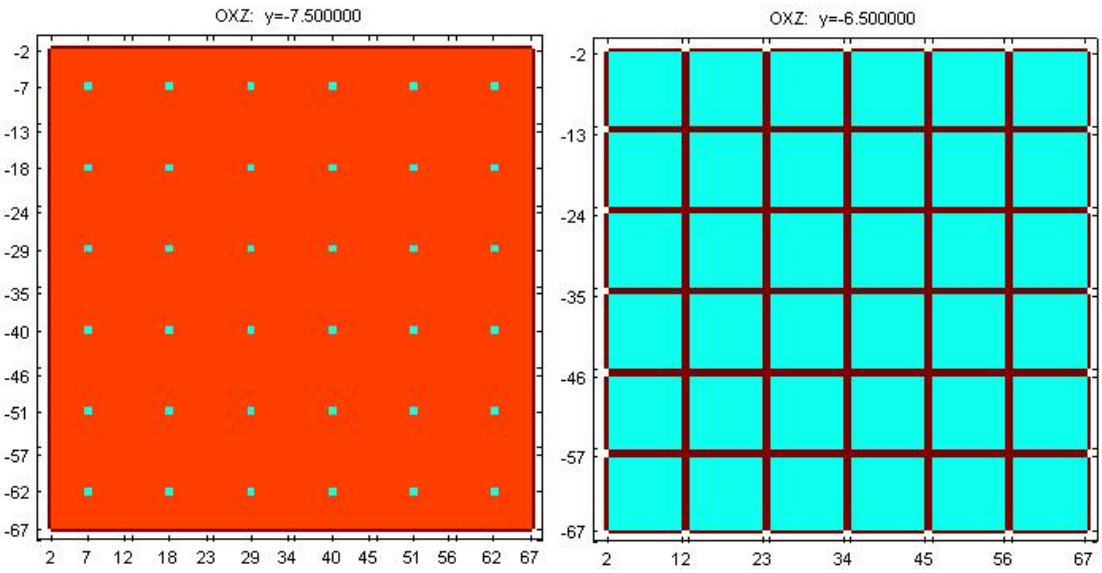

(a) (b)

Figure 10: Cross sectional view of the complicated structure of the multiple porous layers in the channel filter.

nation: 1/0.5 and 1/0.25 mm. Calculations were done with different number of additional fluid layers l, Reynolds number Re, and accuracy ϵ used for solution of auxiliary problems. We show the obtained values of upscaled permeability K_{22} for one of the quasi-porous cells, CPU time T_{SG} of preprocessing step and the total solver time T_{total} (i.e. including the CPU time of subsequent solution on the coarse 1 mm grid), and finally the global pressure drop dP. The maximal memory used by the solver in all cases was 26.68 MB (coarse grid solver + upscaled permeability tensors).
The results show that the additional number of layers (oversampling) is an essential parameter in our case. Also, the choice of the coarse grid is important for the selection of quasi-porous cells.

4.6. Simulation of Industrial Filters - Pleated filter

Lastly, another example of a real filter with complicated filter media is considered. Figure 12 shows a pleated filter geometry on coarse and fine grids. The coarse grid does not resolve the shape of the filtering medium properly. Our aim is to solve the problem using equation 2 on the coarse grid, and employ the subgrid algorithm described in Section 3 to compute the $\tilde{K}_{eff}$

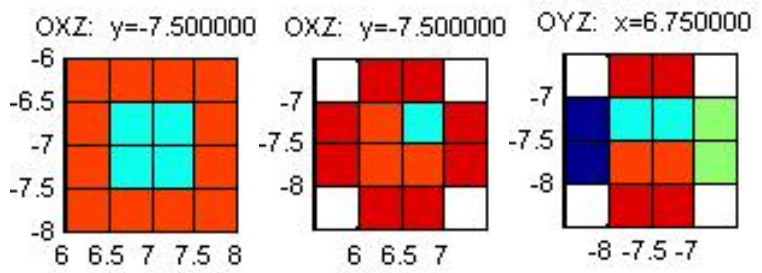

(a) (b) (c)

Figure 11: Resolution of one of the holes in first porous layer

Grid resolution	Number of CVs	Memory [MB]	CPU time [s]	Pressure drop [kg/(mm s^2)]
2 mm	5445	4.42	63.54	16.762
1 mm	37400	26.49	465.02	11.627
0.5 mm	299200	182.70	28271.47	1.579
0.25 mm	2393600	1338.37	518425.0	1.762

Table 4: Simulation results for channel filter with multiple porous layers using the single grid algorithm.

for selected quasi-porous cells. Figure 12 (c) also illustrates the quasi-porous block on which fine scale auxiliary problem is solved. It should be noted that the number of cells in this block are fairly less compared to solving the fine scale problem on the complete filter element. In fact, computing permeability from simulation in a significantly smaller block gives the same results. In the case when all the pleats are of the same size, and the distances between them are equal, it is possible to consider only one smaller block, containing one pleat, to calculate the permeability for this block, and after that to assign this permeability to each coarse cell in the quasi-porous block from 12, which contains all the pleats.

In Table 6, we present the results of solving this problem with the single grid numerical algorithm for two different grid resolutions. The coarse scale is of 1mm size and fine scale resolution is $0.5mm$. The results illustrate the extent to which the computational time for solving a complete problem could increase with finer grid resolutions. Almost 100 times more computational

Scales	l	K_{22}	T_{SG}	T_{total}	dP
1/0.5 mm	1	0.01092	54.8	781.5	1.6919
1/0.5 mm	2	0.01177	93.4	838.3	1.6289
1/0.25 mm	1	0.00588	883.3	1502.9	2.3862
1/0.25 mm	2	0.00863	787.7	1464.8	1.9173
1/0.25 mm	3	0.00960	993.0	1692.1	1.8101
1/0.25 mm	4	0.00972	1126.3	1829.4	1.7984

Table 5: Simulation results for channel filter with combi layers (obtained with Subgrid algorithm). l is the number of additional fluid layers used for auxiliary problems. K_{22} is the upscaled permeability in flow direction obtained for one of the quasi-porous cells. T_{SG} is CPU time of preprocessing step. T_{total} is the total CPU time. dP is obtained global pressure drop.

Figure 12: Pleats in the filter on different grids. Fine grid resolves the geometrical shape of the filter and the pleats, where as the coarse grid does not. Subgrid treats all pleats as a block of filtering medium with upscaled permeability computed using fine scale algorithm.

time is required for a problem that is twice finer in grid resolution. Note that different resolutions result in different geometries. For the coarse grid, not only are the shapes of the pleats not correctly accounted for, but also the inlet and outlet are not separated by the porous medium. In fact, the solution is sought for different geometries and for obvious reasons, the pressure drop on the coarse grid is an over estimation.

Grid	dP $(mbar)$	T_{SG}	T_{total} (s)
1mm	2700	-	1421
0.5mm	1874	-	149102
subgrid-1mm-0.5mm	1760	63580	1420

Table 6: Results for geometries described in Figure 12.

Note that the subgrid algorithm is employed as a preprocessing step for the

single grid algorithm. Moreover, in industry, the subgrid method benefits from the fact that for each fixed geometry, many simulations are done using different physical parameters, such as density, viscosity, inflow velocities etc. for assessing the filter performance. In this case, the subgrid method can be used only once and precomputed upscaled permeabilities for the quasi-porous cells/blocks can be further used in subsequent simulations.

5. Summary

A subgrid method is considered as a computational method for achieving desired accurate solutions for our problem. It is mainly employed for cases where the coarse computational grid is unable to accurately account for the complicated geometry and/or the filter media. The single grid algorithm is used as the building block for solving auxiliary problems on the quasi-porous cells and for solving the global coarse scale problem, with special emphasis based on re-usability of solvers. The method emphasizes on the determination of upscaled quantities for use in subsequent coarse scale global simulations. Fine scale solution is sought only on some quasi-porous cell/s or collectively on a block (a collection of coarse cells). The results were presented for the computer simulation experiments using three dimensional models of oil filters. It is observed that the cell/block permeability is strongly influenced by the resolving grid. The CPU time and memory usage is reduced significantly using the subgrid method with the resulting desired accuracy of the pressure drop, which characterizes the flow through filters.

[1] A. Kumar, Numerical Estimation of Surface Parameters by Level Set Methods, PhD Thesis, Technical University of Kaiserslautern, 2003.

[2] A. J. Chorin, Numerical Solution of Navier-Stokes equation, Mathematics of Computation 22 (1968), 745-760.

[3] A. F. Gulbransen, V.L. Hauge, K.A. Lie, A Multiscale Mixed Finite Element Method for Vuggy and Naturally Fractured Reservoirs, 21st Nordic Seminar on Computational Mechanics, Trondheim, 149-152, 2008.

[4] C.A.J. Fletcher, Computational techniques for fluid dynamics. Springer, Berlin etc., 1991.

[5] G. Bonfigli, P. Jenny, An efficient multi-scale poisson solver for the incompressible navier-stokes equations with immersed boundaries. J. Comp. Phys., 228(12), 2009.

[6] G. Allaire, Homogenization of the Navier-Stokes equations in open sets perforated with tiny holes. i: Abstract framework, a volume distribution of holes, Arch. Ration. Mech. Anal. 113 (1991), no. 3, 209-259.

[7] H.C. Brinkman, A calculation of the viscous force exerted by a flowing fluid on a dense swarm of particles, Appli. Sci. Res., t. A1, (1947), 27-34.

[8] H. Hajibeygi, G. Bonfigli, M. A. Hesse, and P. Jenny. Iterative multiscale finite-volume method. J. Comp. Phys., 227(19):8604-8621, Oct 2008.

[9] J. Willems, Numerical Upscaling for Multiscale Flow Problems, PhD thesis, Technical University of Kaiserslautern, 2009.

[10] K. R. Rajagopal, On a hierarchy of approximate models for flows of incompressible fluids through porous solids, Math. Models Meth. Appl. Sci., 17 (2007), 215-252.

[11] L.J. Durlofsky, Numerical calculation og equivalent grid block permeability tensors for heterogeneous porous media, Water Resources Research 27, 669-708, 1991.

[12] M. Kaviany, Principles of Heat Transfer in Porous Media. Springer, New York etc., 1991.

[13] M. Dedering, W. Stausberg, O. Iliev, Z. Lakdawala, R. Ciegis, V. Starikovicius, On new Challenges for CFD Simulation in Filtration, Proceedings of World Filtration Congress, Leipzig, 2008.

[14] O. Iliev, Z. Lakdawala, R. Ciegis, V. Starikovicius, M. Dedering, P.Popov, Advanced CFD simulation of filtration processes, Proceedings of Filtech, Wiesbaden, 2009.

[15] O. Iliev, V. Laptev, On numerical simulation of flow through oil filters. Comput. Vis. Sci., **6** (2004) 139–146.

[16] O. Iliev, V. Laptev, D. Vassileva, Algorithms and software for computer simulation of flow through oil filters. Proc. FILTECH Europa, 2003, Düsseldorf, pp.327–334.

[17] O. Iliev, R.D. Lazarov, and J. Willems, Fast numerical upscaling of heat equation for fibrous materials, J. Computing and Visualization in Science, 2009.

[18] Ph. Angot, Analysis of singular perturbations on the Brinkman problem for fictitious domain models of viscous flows. Math. Meth. Appl. Sci., **22** (1999) 1395–1412.

[19] P. Gresho, R. Sani, *Incompressible flow and the finite element method. Volume 1: Advection-diffusion and isothermal laminar flow*. In collaboration with M. S. Engelman. Chichester: Wiley. 1044 p. (1998).

[36] M. Griebel and M. Klitz. *Homogenisation and Numerical Simulation of Flow in Geometries with Textile Microstructures*. SIAM MMS, 2009. Submitted. Also available as SFB611 preprint no 404 / 2008.

[21] P. Jenny and I. Lunati. Multi-scale finite-volume method for elliptic problems with heterogeneous coefficients and source terms. Proc. Appl. Math. Mech., 6(1):485-486, 2006.

[22] R. Ciegis, O. Iliev, Z. Lakdawala, On parallel numerical algorithms for simulating industrial filtration problems. Computational Methods in Applied Mathematics 7(2), 118-134(2007).

[23] T.Y. Hou, Y. Efendiev, Multiscale Finite Element Methods. Surveys and Tutorials in the Applied Mathematical Sciences, Band 4, Springer, 2009.

[24] T. Arbogast, Analysis of a two-scale, locally conservative subgrid upscaling for elliptic problems, SIAM J. Numer. Anal. 42 (2004), no. 2, 576598.

[25] T. Arbogast, S. L. Bryant, A two-scale numerical subgrid technique for waterflood simulations, SPE Journal 7 (2002) 446-457.

[26] T. Arbogast, Implementation of a locally conservative numerical subgrid upscaling scheme for two-phase Darcy flow, Computational Geosciences 6, 453-481, 2002.

[27] U. Hornung. *Homogenization and porous media*, Springer Verlag New York Inc., New York, USA, 1996.

[28] V. Starikovicius, R. Ciegis, O. Iliev, Z.Lakdawala, A parallel solver for the 3D Simulation of Flows through Oil Filters, Springer Optimization and its applications, Volume 27, 181-191(2008).

[29] V.V. Jikov, S.M. Kozlov, Oleinik O.A., Homogenization of Differential Operators and Integral Functionals, Springer-Verlag, Berlin, 1994.

[30] V. Laptev, Numerical solution of coupled flow in plain and porous media. PhD thesis, Technical University of Kaiserslautern, 2003.

[31] X.H. Wu, Y. Efendiev and T.Y. Hou, *Analysis of upscaling absolute permeability.* Discrete Contin. Dyn. Syst., Series B 2, No. 2, 185-204 (2002).

[32] Y. Chen, L.J. Durlofsky, M. Gerritsen, X.H. Wen, A Coupled Local-Global Upscaling Approach for Simulating Flow in Highly Heterogeneous Formations, Advances in Water Resources, 26, 1041-1060 2003.

[33] Y. Jung, S. Torquato, Fluid permeabilities of triply periodic minimal surfaces, Physical Review Em 72, 056319, 2005.

[34] A. Sangani, A.Acrivos, Int. J. Multiphase Flow, 8, 343, 1982.

[35] James H. Bramble and Joseph E. Pasciak, 1988. A preconditioning technique for indefinite systems resulting from mixed approximations of elliptic problems. Math. Comp., 50(181): 1-17.

[36] M. Griebel, M. Klitz. Homogenisation and Numerical Simulation of Flow in Geometries with Textile Microstructures. SIAM MMS, 2009.